NATIONAL RADIO ASTRONOMY OBSERVATORY
Charlottesville, Virginia 22903

MMA MEMORANDUM # 103
(also distributed as EDIR No. 295)

Some Fundamental and Practical Limits on Broadband Matching to Capacitive Devices, and the Implications for SIS Mixer Design

A. R. Kerr

September 30, 1993

CONTENTS

Some Fundamental and Practical Limits on Broadband Matching to Capacitive Devices, and the Implications for SIS Mixer Design

A. R. Kerr

ABSTRACT

In a given frequency band, the achievable match between a capacitive microwave or millimeter-wave device and a resistive source is limited by the capacitance of the device and its series inductance. The fundamental limit on the match bandwidth is examined for three circuits: (i) parallel RC, (ii) parallel RC with series L, and (iii) parallel RCL with series L. The broadband matching theories of Bode (1945) and Fano (1950) are used, the latter modified to avoid the standard low-pass to band-pass mapping in case (ii) because the terminals of the capacitance are not generally accessible for connection of the requisite parallel inductor. The results are fundamental to the design of broadband mixers, multipliers, switches, and detectors using Schottky diodes or SIS junctions.

Practical limitations imposed by the minimum realizable dimensions of millimeter-wave integrated circuits fabricated by standard photolithography are discussed in the context of SIS mixers with series arrays of junctions, and an example of a coplanar SIS mixer design is given. For a series array of N devices with a given total resistance, it is shown that there is an upper limit to N, below which the theoretical match bandwidth depends only on the RC product of the devices and not on the series inductance of the array.

I. Introduction

Many semiconductor and superconductor devices are inherently capacitive and can be well described by the parallel RC circuit shown in Fig. 1(a). This is true of Schottky diodes and SIS superconducting quasi-particle tunnel junctions at frequencies up to several hundred GHz. In many practical cases the geometry of the device adds an unavoidable series inductance, as indicated in Fig. 1(b). In either case, the bandwidth over which it is possible to couple power efficiently to the device from a resistive source can be increased, often considerably, by inserting a lossless matching network between the source and the device. In some cases, it is possible to connect an inductive tuning element directly across the terminals of the intrinsic device, as shown in Fig. 1(c). The purpose of the present work is to determine the fundamental match-bandwidth limits of these circuits. Specifically, in sections II-V, we determine the lowest upper bound on the magnitude of the reflection coefficient that can be achieved over a given frequency band. This is illustrated in Fig. 2, where it is required that $|\rho| \le \rho_a$ within the frequency band $\omega_1 \le \omega \le \omega_2$, but can have any value outside that frequency range. The resulting minimum possible value of ρ_a is of fundamental importance in the design of broadband circuits incorporating SIS junctions or semiconductor diodes.

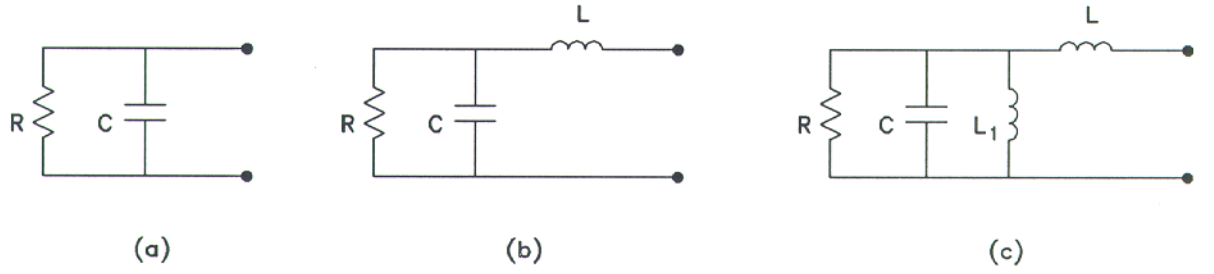

Fig. 1. Equivalent circuits of: (a) a capacitive device, (b) a capacitive device with series inductance, and (c) an inductively tuned device with series inductance.

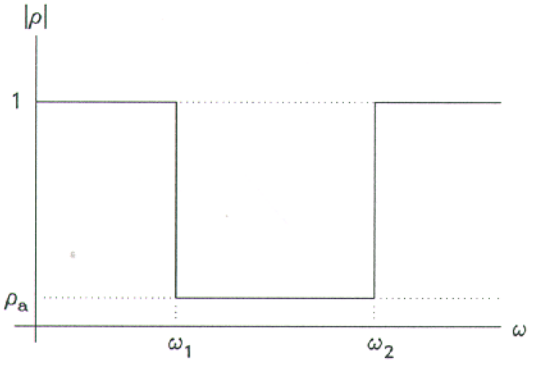

Fig. 2. $|\rho|$ is required to lie below the solid curve. The minimum possible value of ρ_a, in the given frequency band ω_1 and ω_2, is to be determined.

This work uses the well-known broadband matching theory, published in 1945 and 1950, of Bode [1] and Fano [2]. In their work, the conditions of physical realizability were used to derive limits on the voltage reflection coefficient of a given load with an arbitrary lossless matching network. In section II of this paper, Bode's match-bandwidth limit is applied to the circuit of Fig 1(a). In sections III and IV, the theory of Fano is used to derive limits for the circuits of Fig. 1(b) and (c). For the case of Fig. 1(b), this requires a slight modification to the theory to cover the case of band-pass matching without the use of the usual low-pass to band-pass mapping. Section V presents the theoretical bandwidth limits for the three circuits of Fig. 1 in graphical form. It is apparent that the series inductance of a device limits the bandwidth of a circuit only when it exceeds a certain value which depends on R and C.

Section VI discuses the implications of the match-bandwidth limits for practical double-sideband mixers, using broadband SIS mixers as examples. Sections VII and VIII examine the practical constraints on the series inductance of devices and series arrays of devices in coplanar waveguide

circuits, and give an example of a broadband coplanar SIS mixer with an array of junctions. For circuits using series arrays of devices, it is shown that there is no trade-off between the attainable bandwidth and the number of devices in the array so long as the number of devices does not exceed a critical value.

II. The Capacitive Device

In the case of the simple circuit of Fig. 1(a), connected via a lossless matching network to a resistive source, Bode [1] showed that the reflection coefficient ρ is constrained by the integral equation:

$$\int_0^\infty \ln|1/\rho(\omega)|.d\omega \leq \pi/RC \ . \tag{1}$$

Inspection of (1) indicates that the lowest value of the upper bound of $|\rho|$ (ρ_a in Fig. 2) within the frequency band $\omega_1 \leq \omega \leq \omega_2$ is achieved when $|\rho| = \rho_a$ within that band, and $|\rho| = 1$ at all other frequencies. The optimum $|\rho(\omega)|$ therefore coincides with the solid curve in Fig. 2. The integral in (1) is then simply evaluated, giving

$$\ln(1/\rho_{a,min}) = \pi/RC(\omega_2 - \omega_1) \ . \tag{2}$$

It is apparent that $\rho_{a,min}$ depends on the desired bandwidth $(\omega_2 - \omega_1)$ but not on the location of the band along the frequency axis.

III. The Capacitive Device with Series Inductance

Fano [2] extended the work of Bode to include a more general load equivalent circuit for the case of low-pass matching (*i.e.*, for $\omega_1 = 0$ in Fig. 2). This can be applied to the case of band-pass matching by using the standard low-pass to band-pass mapping, $\omega \rightarrow \omega_x(\omega/\omega_x - \omega_x/\omega)$, which transforms all inductors and capacitors in the circuit into series or parallel LC resonators. However, this transformation is not applicable to the device described by Fig. 1(b), as the terminals of the capacitor are not accessible for connection of a parallel inductor. The procedure of Fano is applied below, modified slightly to avoid using a low-pass to band-pass transformation, to determine the lowest possible value of the upper bound of the magnitude of the reflection coefficient within a given frequency band, for the circuit of Fig. 1(b).

The given device and its external matching circuit are depicted in Fig. 3. Following Fano, the best possible match over a specified frequency band is deduced from consideration of the function $F(s) = \ln(1/\rho_1(s))$, where $s = \sigma + j\omega$ is the complex frequency variable. Expanding F(s) as a Taylor series in 1/s:

$$F(s) = \ln(1/\rho_1) = jA_0 + A_1(1/s) + A_3(1/s)^3 + \ldots \tag{3}$$

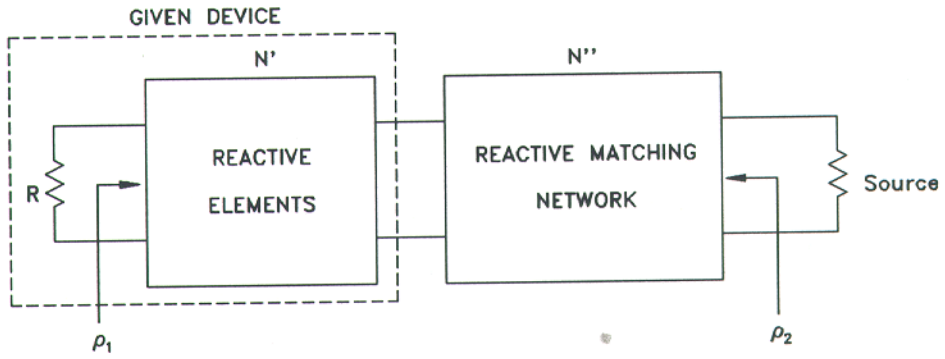

Fig. 3. The load R and network N' are part of the given device. Network N'' contains reactive matching elements.

The coefficient A_0 is equal to 0 or π, while the other A_n must all be real, since $|\rho_1|$ is an even function of ω and $\arg(\rho_1)$ is an odd function of ω. Fano showed [2, pp. 62-63] that, since the m transmission zeros of N' must also be transmission zeros of the whole circuit (N' + N"), it follows that, except in the degenerate case discussed below, ρ_1 and its first (2m-1) derivatives, evaluated at the transmission zeros of N', are independent of the matching network N". The same is true of $\ln(1/\rho_1)$ and its derivatives. The first 2m Taylor coefficients, $A_n = (1/n!)d^nF(s)/d(1/s)^n$, can therefore be evaluated from a knowledge only of the equivalent circuit of the given device.

If the left-hand element of N" is of the same type (L or C) and orientation (series or parallel) as the right-hand element of N', the circuit is said to be *degenerate*. N' and N" then have a common transmission zero and only (2m-2) derivatives of ρ_1 are independent of N" [2, pp. 71-73].

Now consider the circuit of Fig. 1(b), terminated on the right by an arbitrary resistance, as shown in Fig. 4. For convenience, the values of the circuit elements are impedance-scaled to R = 1 ohm (the impedance level has no effect on reflection coefficient or matching bandwidth). The network N' has two zeros of transmission, due to C and L, both at $s = \infty$, so m = 2. Then,

$$Z_1' = \frac{sL + r}{s^2LC + srC + 1} \tag{4}$$

and

$$\frac{1}{\rho_1} = \frac{Z_1' + 1}{Z_1' - 1} = -\frac{s^2LC + s(L+rC) + (1+r)}{s^2LC - s(L-rC) + (1-r)} \; . \tag{5}$$

In terms of the variable $\xi \triangleq 1/s$,

$$\ln[\frac{1}{\rho_1}] = \ln[-\frac{\xi^2(1+r) + \xi(L+rC) + LC}{\xi^2(1-r) - \xi(L-rC) + LC}] \; . \tag{6}$$

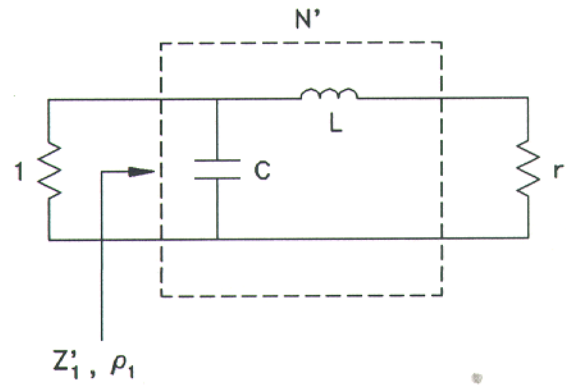

Fig. 4. The network N', for the circuit of Fig. 1(b), arbitrarily terminated on the right. Values of the circuit elements are impedance-scaled to R = 1 ohm.

The first 2m Taylor coefficients A_n are obtained from the derivatives of $\ln(1/\rho_1)$ evaluated at $\xi = 0$, and are independent of the arbitrary resistance r as expected:

$$jA_0 = j\pi \ , \qquad A_1 = \frac{2}{C} \ , \qquad A_2 = 0 \ , \quad \text{and} \quad A_3 = \frac{2}{3}\,\frac{L - 3C}{LC^3} \ . \tag{7}$$

When the network N' in Fig. 3 has two transmission zeros at $s = \infty$, Fano showed that, in the non-degenerate case, physical realizability of the matching network N" requires the following integral equations to apply:

$$\int_0^\infty \ln\left|\frac{1}{\rho_1}\right| d\omega = \frac{\pi}{2}\,(A_1 - 2\,\Sigma\,\lambda_{ri}) \tag{8}$$

and

$$\int_0^\infty \omega^2 \ln\left|\frac{1}{\rho_1}\right| d\omega = -\frac{\pi}{2}\,(A_3 - \frac{2}{3}\,\Sigma\,\lambda_{ri}^3) \ , \tag{9}$$

where $\lambda_{ri} = \sigma_{ri} + j\omega_{ri}$ are the zeros of ρ_1 that lie in the right half of the s-plane, and depend on both networks N' and N" in Fig. 3. In the degenerate case, eq. (8) alone is required.

The upper bound on $|\rho_1|$ is minimized if the matching network N" is chosen so that within the pass band, $\omega_1 \le \omega \le \omega_2$, $|\rho_1|$ is equal to the upper bound ρ_a, while outside the pass band $|\rho_1| = 1$, as depicted by the solid curve in Fig. 2. With this form of $\rho_1(\omega)$, the integrals in (8) and (9) can be evaluated, giving

$$(\omega_2 - \omega_1)\ln|1/\rho_a| = (\pi/2)(A_1 - 2\,\Sigma\,\lambda_{ri}) \tag{10}$$

and

$$(\omega_2^3 - \omega_1^3)\ln|1/\rho_a| = -(\pi/2)(3A_3 - 2\,\Sigma\,\lambda_{ri}^3) \ . \tag{11}$$

These band-pass equations are similar to Fano's low-pass equations [2, eqs. (25) and (26)]. In the degenerate case, eq. (10) alone is required.

The remaining step is to find the right half-plane zeros λ_{ri} of ρ_1 in (10) and (11) that maximize $\ln|1/\rho_a|$ (*i.e.*, minimize ρ_a) for a given pass band, ω_1 to ω_2. Following the argument used by Fano for the non-degenerate low-pass case ($\omega_1 = 0$), it is evident that to maximize $\ln|1/\rho_a|$ the matching network must be selected so that $\Sigma\ \lambda_{ri}^3$ is as large as possible while keeping $\Sigma\ \lambda_{ri}$ as small as possible. This is accomplished by using a single real zero, σ_r [2, p. 72]. Then, from (10) and (11),

$$(\omega_2 - \omega_1)\ln|1/\rho_a| = (\pi/2)(A_1 - 2\sigma_r) \tag{12}$$

and

$$(\omega_2^3 - \omega_1^3)\ln|1/\rho_a| = -(\pi/2)(3A_3 - 2\sigma_r^3)\ . \tag{13}$$

Eliminating σ_r between these equations, and putting $K = (2/\pi)\ln(1/\rho_{a,min})$, gives

$$K(\omega_2^3 - \omega_1^3) + 3A_3 - (1/4)[A_1 - K(\omega_2 - \omega_1)]^3 = 0\ , \tag{14}$$

which is a cubic equation in K.

It is convenient at this point to change the frequency variables from ω_1 and ω_2 to the center frequency ω_0 and fractional bandwidth b. Substituting $\omega_1 = \omega_0(1 - b/2)$ and $\omega_2 = \omega_0(1 + b/2)$ in (14) gives

$$\omega_0^3 b^3 K^3 - 3\omega_0^2 b^2 A_1 K^2 + \omega_0 b\ [\omega_0^2 b^2 + 12\omega_0^2 + 3A_1^2]\ K + [12A_3 - A_1^3] = 0\ . \tag{15}$$

Substituting the values for A_1 and A_3 from (7), and putting $X_L = \omega_0 L$ and $B_C = \omega_0 C$, gives

$$K^3 - \frac{6}{bB_C}K^2 + \frac{1}{b^2B_C^2}[12B_C^2 + 12 + b^2B_C^2]\ K - \frac{24}{b^3X_LB_C^2} = 0\ , \tag{16}$$

which can be solved for K.

In the degenerate case, the first element of the optimum matching network is inductive, thereby augmenting L. Equation (10) alone is then required, for which $\ln|1/\rho_a|$ is maximized when ρ_1 has no right-half-plane zeros; *i.e.*, $\Sigma\ \lambda_{ri} = 0$. Using $A_1 = 2/C$ from (7), (10) becomes identical to the Bode limit of eq. (2). In terms of K, b, and B_C, the Bode limit is given by:

$$K = \frac{2}{bB_C}\ . \tag{16a}$$

IV. The Inductively Tuned Device with Series Inductance

For an inductively tuned device with series inductance, as in Fig. 1(c), the standard low-pass to band-pass mapping allows the fundamental limit on the match bandwidth to be deduced from the low-pass case. The low-pass prototype is simply the circuit of Fig. 1(b). Equations (12) and (13) are used, with $\omega_1 = 0$, whence

$$\omega_2 K = A_1 - 2\sigma_r \tag{17}$$

and

$$\omega_2^3 K = -3A_3 + 2\sigma_r^3 \ . \tag{18}$$

Eliminating σ_r between these equations, and substituting for A_1 and A_3 from (7), gives

$$K^3 - \frac{6}{\omega_2 C} K^2 + [\frac{12}{\omega_2^2 C^2} + 4]K - \frac{24}{\omega_2^3 C^2 L} = 0 \ , \tag{19}$$

which can be solved for $K(\omega_2)$.

We now use the low-pass to band-pass mapping

$$\omega \rightarrow \omega_x[\frac{\omega}{\omega_x} - \frac{\omega_x}{\omega}] \ , \tag{20}$$

where $\omega_x = 1/\sqrt{(L_1 C)}$ is the resonant frequency of all the LC resonators in the transformed (band-pass) circuit. Low-pass and band-pass circuits related by (20) have equal bandwidths. Since the low-pass circuit under consideration has a bandwidth equal to ω_2 (*i.e.*, $\omega_1 = 0$ in Fig. 2), the fractional bandwidth of the band-pass circuit is $\beta = \omega_2/\omega_x$. Substituting $\omega_2 = \beta\omega_x$ in (19) gives

$$K^3 - \frac{6}{\beta\omega_x C} K^2 + [\frac{12}{\beta^2\omega_x^2 C^2} + 4]K - \frac{24}{\beta^3\omega_x^3 C^2 L} = 0 \ . \tag{21}$$

The fractional bandwidth β used here differs in definition from the fractional bandwidth b used in Section III. If the band edge frequencies are ω_a and ω_b, then $\beta = (\omega_b - \omega_a)/\omega_x$, while $b = (\omega_b - \omega_a)/\omega_0$, where the mean frequencies $\omega_x = \sqrt{(\omega_a\omega_b)}$ and $\omega_0 = (\omega_a + \omega_b)/2$. To facilitate comparison between results for the different equivalent circuits in the next section, it is necessary to change the variables β and ω_x, in (21) to b and ω_0 using $\beta = b/\sqrt{(1 - b^2/4)}$ and $\omega_x = \omega_0\sqrt{(1 - b^2/4)}$. Writing $B_C = \omega_0 C$, and $X_L = \omega_0 L$ gives

$$K^3 - \frac{6}{bB_C} K^2 + [\frac{12}{b^2 B_C^2} + 4]K - \frac{24}{b^3 B_C^2 X_L} = 0 \ . \tag{22}$$

In the degenerate case, when the first element of the optimum matching network is inductive, the Bode limit applies and is given by the low-pass to band-pass mapping of eq. (2) according to eq. (20). The result is identical to eq. (16a), *viz.*,

$$K = \frac{2}{bB_C} \quad . \tag{22a}$$

V. Results and Discussion

It is not usually known in advance whether a particular circuit of the form of Fig. 1(b) or (c), connected to its optimum matching network, will be degenerate or not. If degenerate, the series inductance L does not exceed some limiting value, L_B, below which the match bandwidth is limited only by C. The Bode limit then is attainable, and eq. (16a) or (22a) is applicable. If, on the other hand, the optimally matched circuit is non-degenerate, then $L > L_B$, and the match bandwidth is limited by C *and* L; eq. (16) or (22) is then appropriate. In the present work, however, this uncertainty does not present an obstacle; the equations for both cases are solved, the correct solution being the more restrictive one as is clear from the graphical results below.

The parameters $X_L = \omega_0 L$ and $B_C = \omega_0 C$ in eqs. (16), (16a), (22), and (22a) apply to the circuits of Fig. 1(b) with impedances scaled to R = 1. For the unscaled circuit, they become:

$$X_L = \frac{\omega_0 L}{R} \qquad \text{and} \qquad B_C = \omega_0 RC \quad . \tag{23}$$

Equations (16), (16a), (22), and (22a) have been solved for a range of values of X_L and B_C. As the present work was done in the context of SIS mixer design, values of X_L and B_C appropriate to SIS mixers are used in the examples below. It should be noted that B_C is not the familiar $\omega_0 R_N C_J$ product of the SIS junction(s), but is $\omega_0 R_{RF} C_J$, where R_{RF} is the small signal RF input impedance of the mixer. Likewise, $X_L = \omega_0 L / R_{RF}$. (For a well designed SIS mixer, R_{RF} usually lies within a factor of ~3 of R_N; *i.e.*, $R_N/3 \le R_{RF} \le 3R_N$ [3, 4].)

Corresponding to a range of different devices, we have chosen $B_C = \omega_0 RC = 2, 4, 8$, and values of $X_L = \omega_0 L/R$ in the range 0 to 10. The values of the lowest upper bounds, $|\rho_{a,min}|$ on the reflection coefficient, and $1/(1-|\rho_{a,min}|^2)$ on the reflection loss, versus fractional bandwidth b, are shown in Figs. 5 and 6 for the circuits of Figs. 1(b) and 1(c), respectively. The Bode limit for L=0 (*i.e.*, the circuit of Fig. 1(a)) is indicated by the dashed curves. The dotted curves, shown for comparison, are for a parallel RC device tuned by a parallel inductor and connected to a source resistance R, but with no additional matching (*i.e.*, the circuit of Fig. 1(c) with L = 0). The short horizontal lines indicate the values of $|\rho|$ and $1/[1-|\rho|^2]$ at frequency ω_0 for a parallel RC device connected to a source resistance R with no matching elements (*i.e.*, the circuit of Fig. 1(a)).

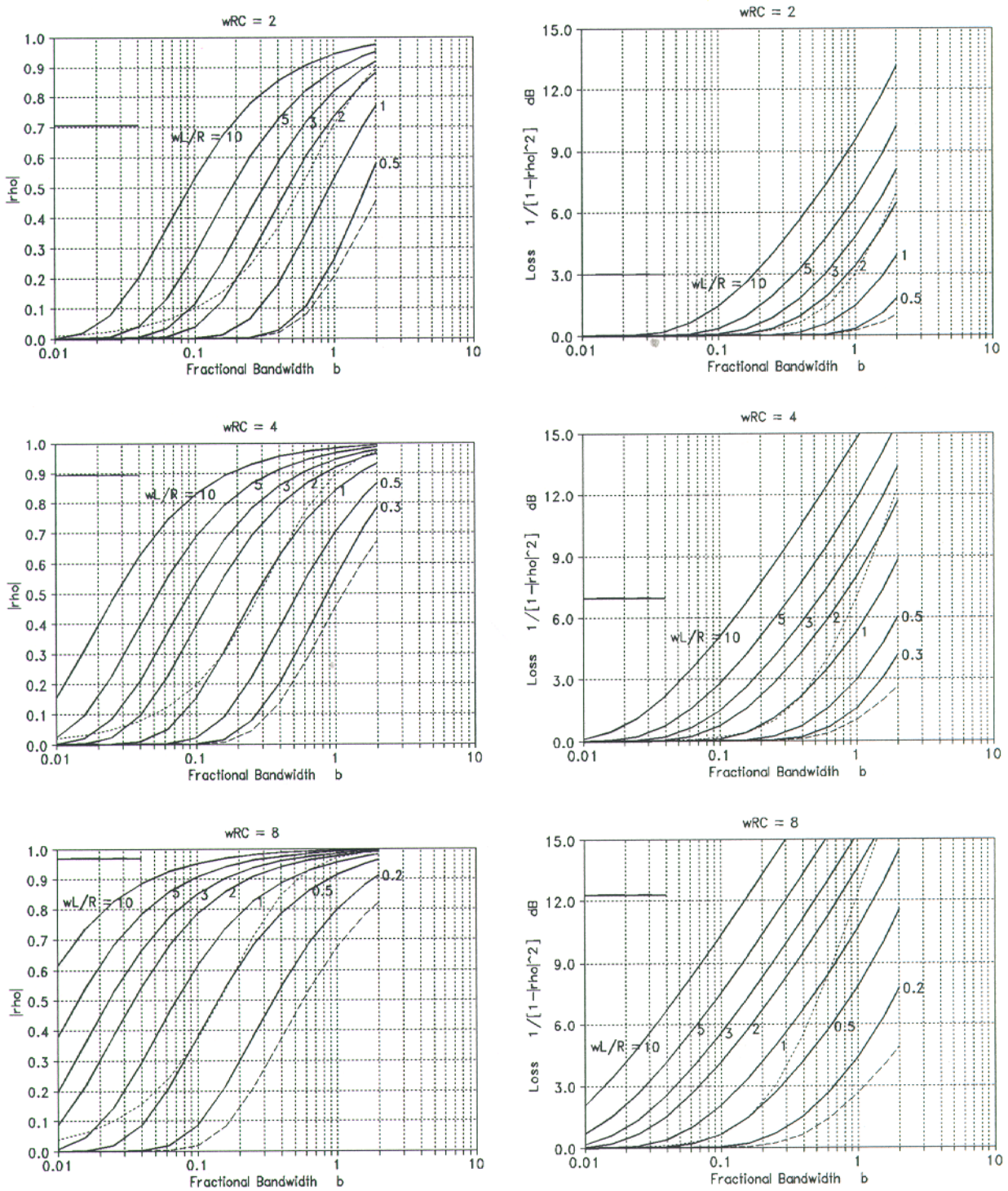

Fig. 5. For the capacitive device with series inductance (Fig. 1(b)), the lowest upper bounds, $|\rho_{a,min}|$ on the reflection coefficient, and $1/(1-|\rho_{a,min}|^2)$ on the reflection loss, *vs* fractional bandwidth b, with $\omega_0 RC = 2$, 4, and 8, and various values of $\omega_0 L/R$. The Bode limit for the case $L = 0$ is indicated by the dashed curves. The dotted curves are for a parallel RC device tuned by a parallel inductor but with no additional matching. The short horizontal lines indicate the values of $|\rho|$ and $1/[1-|\rho|^2]$ at frequency ω_0 for a parallel RC device connected to a source resistance R with no matching.

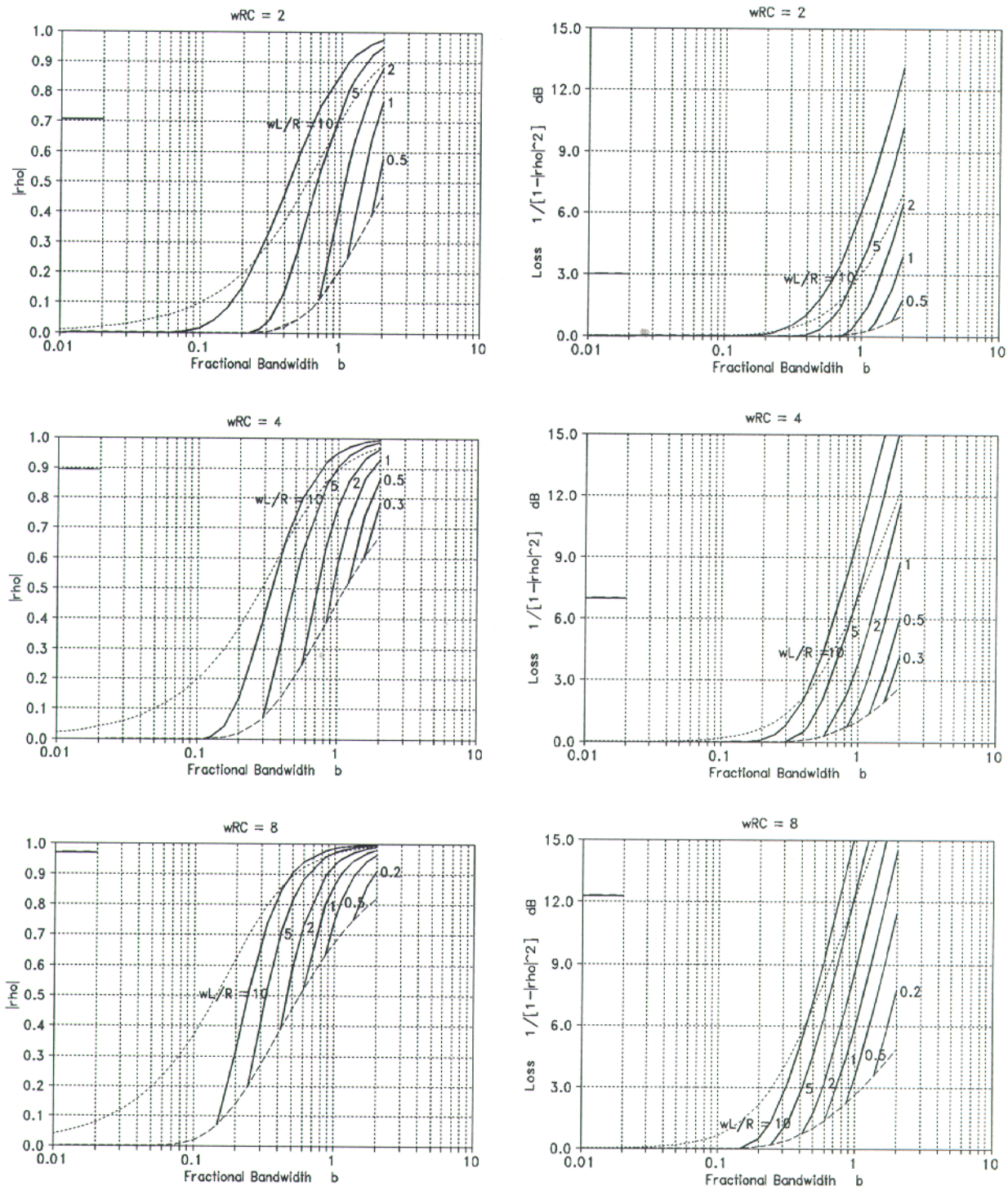

Fig. 6. For the inductively tuned capacitive device with series inductance (Fig. 1(c)), the lowest upper bounds, $|\rho_{a,min}|$ on the reflection coefficient, and $1/(1-|\rho_{a,min}|^2)$ on the reflection loss, *vs* fractional bandwidth b, with $\omega_0 RC$ = 2, 4, and 8, and various values of $\omega_0 L/R$. The Bode limit for the case L = 0 is indicated by the dashed curves. The dotted curves are for a parallel RC device tuned by a parallel inductor but with no additional matching. The short horizontal lines indicate the values of $|\rho|$ and $1/[1-|\rho|^2]$ at frequency ω_0 for a parallel RC device connected to a source resistance R with no matching.

The Bode limit, indicated in Figs. 5 and 6 by the dashed curves, applies when L is less than the quantity L_B, whose value depends on the other elements of the equivalent circuit and the desired bandwidth. When $L \leq L_B$, the match bandwidth is not limited by L, but only by C and R. In this case, the first element of the optimum matching network is a series inductance (L_B-L), effectively augmenting L. This is the degenerate case discussed above. When L exceeds L_B (the non-degenerate case), it too limits the attainable match bandwidth of the circuits, as indicated in the figures.

VI. Application to Mixers

Some caution is required in interpreting the results of Figs. 5 and 6 in the context of matching to double sideband mixers. While the $|\rho|$ curves in these figures indicate the range of variation of the source impedance seen by the intrinsic mixing device (R in Fig. 1), the loss ($1/[1-|\rho|^2]$) curves should not be regarded simply as part of the conversion loss of the mixer which can be eliminated by tuning. This is because the signal frequency input impedance of a mixer depends in part on the image frequency embedding impedance. If the signal and image circuits of the mixer are physically the same, tuning the circuit changes the image termination and therefore the signal frequency input impedance of the mixer. In effect, the device resistance R at the signal frequency becomes a function of the matching circuit, and the minimum conversion loss does not, in general, occur for a matched input.

The dependence of the performance of a typical 230 GHz double sideband SIS mixer receiver on embedding admittance is indicated in Fig. 7, which shows contour plots of the mixer and receiver parameters plotted on Smith charts of RF embedding *admittance* (*i.e.*, in the $(-\rho)$-plane) normalized to the optimum source conductance $1/R_{S,opt}$ ($R_{S,opt}$ is defined in the Appendix). The receiver includes an IF amplifier with T_{IF} = 4 K, and an IF isolator at 4 K. The IF load impedance Z_{IF} is fixed and equal to $R_{S,opt}$. Note that the source (embedding) admittance is defined to include the capacitance of the junction(s), and is assumed equal at the upper and lower sideband frequencies. The mixer gain and receiver noise temperature are shown as single-sideband (SSB) quantities. Further details of the mixer and the method of analysis are given in the Appendix.

Fig. 7 clearly demonstrates three quantum characteristics of SIS mixers that are not possible in classical diode mixers: (i) the (SSB) conversion loss is less than the 3 dB classical limit for a DSB mixer, (ii) the contours are asymmetrical about the real axis, an effect caused by the quantum susceptance of the SIS junction, and (iii) the output resistance can be negative, which is impossible in classical resistive mixers. The significance of the negative output resistance is discussed further below.

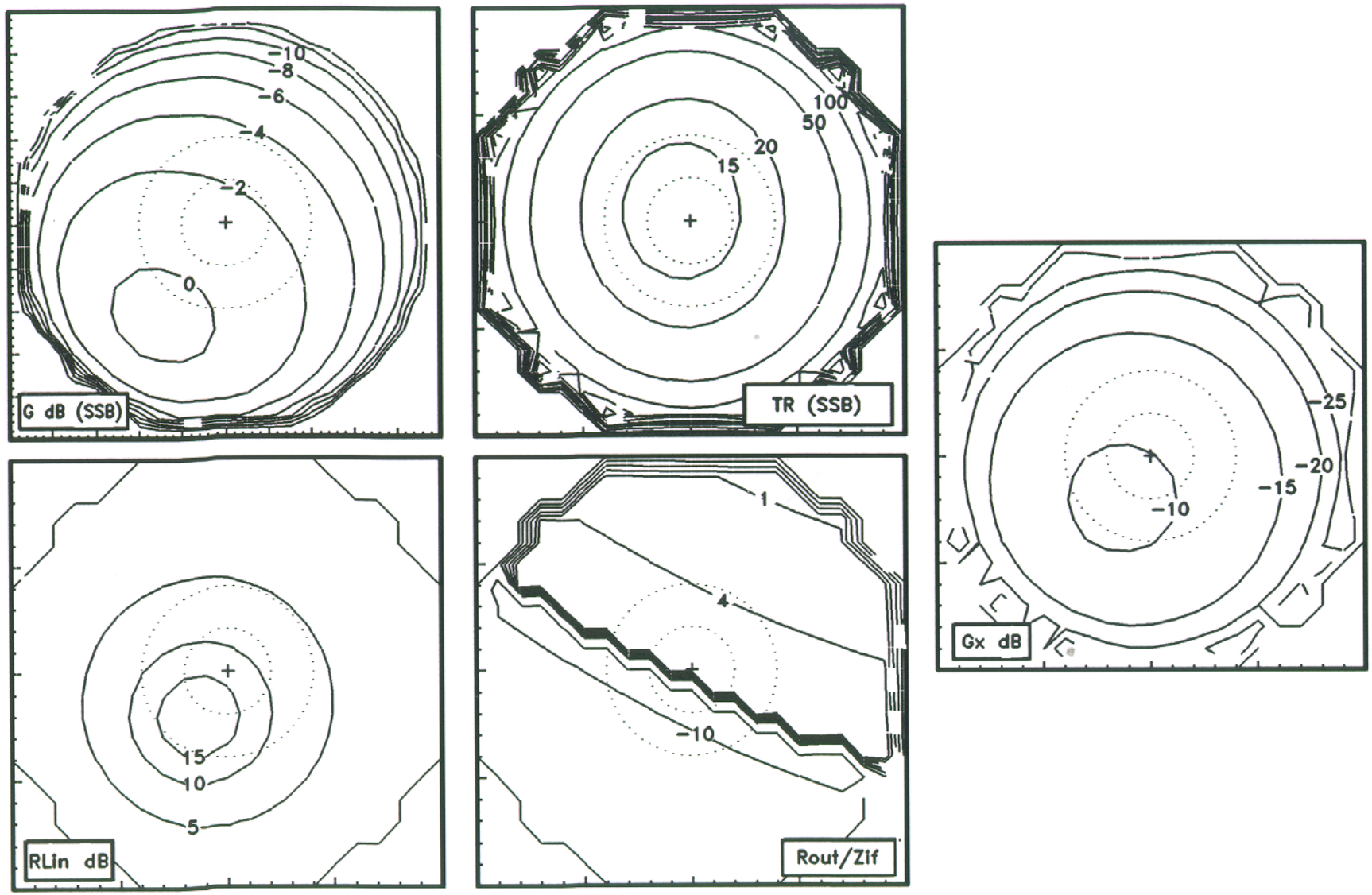

Fig. 7. Contour plots of mixer gain, receiver noise temperature, input return loss, IF VSWR, and signal-to-image conversion gain, for a 230 GHz SIS receiver. The contours are plotted on Smith charts of RF source admittance (*i.e.*, in the $-\rho$ plane). The dotted circles are $|\rho| = 0.2$ and $|\rho| = 0.4$. The receiver includes an IF amplifier with $T_{IF} = 4$ K, and an IF isolator at 4 K. The mixer gain and receiver noise temperature are shown as SSB quantities. (See text for further details.)

The table below summarizes the range of variation of the receiver parameters in Fig. 7 when the embedding admittance falls within the circles $|\rho| = 0.2$ and 0.4 (shown dotted in the figure) over the frequency band of interest. Analysis at other frequencies indicates that the 230 GHz results in the table above are typical of SIS receivers of similar design using Nb junctions at frequencies from 70 to at least 350 GHz. It is clear from the table that even an SIS mixer whose embedding admittance is designed for $|\rho| \leq 0.4$ should have acceptable performance across the intended frequency band for most practical applications.

	$\|\rho\| \leq 0.2$	$\|\rho\| \leq 0.4$
Mixer conversion gain (SSB)	-0.5 → -1.5 dB	+0.5 → -4.0 dB
Receiver noise temp (SSB)	12 → 15 K	12 → 20 K
Input return loss	> 8 dB	> 5 dB
Signal-to-image conv. loss	9 → 11 dB	9 → 13 dB
Output VSWR (R_{out}/Z_{IF})	-17 → +6	-5 → +3

Negative Output Resistance in SIS Mixers

On the contour plot of R_{out}/Z_{IF} in Fig. 7, the transition of the output impedance from a large positive value to a large negative value is quite sudden. However, if the contours were re-plotted as output *conductance*, the transition from positive, through zero, to negative would be quite smooth and continuous, and there is no reason to expect any sudden change in receiver performance as this occurs. Indeed, when tuning a receiver, this transition can often be observed on the pumped I-V curve as the differential conductance at the bias point goes from positive, through zero, to negative. However, under certain conditions, the presence of negative output resistance can have two possibly adverse effects: (i) it can cause (small-signal) instability and oscillation in the RF, IF, or bias circuits, and (ii) in a series array of junctions, negative DC differential resistance can cause instability in the biasing of the junctions and the division of the LO voltage between them. These will be discussed further below. A third possible concern is that noise from the IF amplifier or isolator, incident on the IF port of the mixer, will be reflected with gain back into the amplifier from the negative output resistance of the mixer. This, however, is taken into account in the analysis used to generate Fig. 7.

(i) A device with negative (differential) resistance is potentially unstable. Depending on the device, it may be stable with a high impedance load or with a low impedance, as can be demonstrated by considering series and parallel LRC circuits with negative resistance. (Analysis of the time-domain differential equations describing these circuits shows that the former is stabilized by a high resistance load, and the latter by a low resistance load.) In general, to determine the stability of a negative resistance device connected to a load, the complex impedance of the device and load must be known *at all frequencies*. It is possible, however, to make some general observations about the nature of the stability of mixers with negative resistance. With no LO power applied, an SIS junction (or array) is stable, regardless of the embedding impedance $Z_e(\omega)$, and the reflection coefficient of

the junction (or array) with respect to the embedding impedance, $|\rho_j(\omega)| = |Z_j - Z_e^*|/|Z_j + Z_e| \leq 1$ [1], where $Z_j(\omega)$ is the (small signal) impedance of the junction. As the LO power is increased, it is possible that at some frequency ω_{xx}, $|\rho_j|$ will become infinite; *i.e.*, $Z_j(\omega_{xx}) + Z_e(\omega_{xx}) \rightarrow 0$. Under this condition the circuit is on the point of oscillation, and an impulsive excitation of the junction will cause undamped ringing at frequency ω_{xx}. Because of the mixing action of the junction, this incipient instability occurs simultaneously at ω_{xx} and at all the related sideband frequencies $n\omega_{LO} + \omega_{xx}$, $-\infty \leq n \leq \infty$, at each of which $|\rho_j| \rightarrow \infty$. Clearly, as the LO power is increased from zero, *instability is preceded by high reflection gain and conversion gain at a complete set of related sideband frequencies*, but not necessarily within the *normal* signal, image, and IF bands. In practice, one can only ensure that, as the LO power is increased from zero to the operating level (usually $\alpha \simeq 1$), the gain does not become large within the normal IF band, for which the signal, image, and IF embedding impedances are known. In the region of negative IF output resistance in Fig. 7, for example, the magnitude of $|R_{out}/Z_{IF}| \geq 1.9$ almost to the edge of the Smith chart, and no instability would be expected at frequencies where the IF load impedance Z_{IF} remains near its nominal value. Instability could occur far above the IF band if the bias-T, circulator, or amplifier exhibited a resonance which would allow $Z_j(\omega_{xx}) + Z_e(\omega_{xx}) = 0$ to be satisfied. For the broadband SIS mixers reported to date, this has not, apparently, been a problem.

(ii) The second and least predictable effect of negative resistance has been observed in fixed-tuned SIS mixers using series arrays of SIS junctions [4]. It is suspected that negative DC differential resistance in a series array can cause an unstable situation in which the individual junctions become unequally biased and unequally driven by the LO. Ultimately, a stable dynamic state is reached in which the junctions remain unequally biased and driven. As this instability appears to be avoided in mechanically tunable mixers using arrays of SIS junctions with integrated tuning circuits, similar to those used in [4], we surmise that it can be avoided by appropriate design of the embedding impedance as a function of frequency.

VII. Practical Constraints on the Series Inductance

For integrated circuits, such as mixers, multipliers, switches, and modulators, in the ~100-400 GHz range, several basic circuit configurations are possible. These include waveguide mounts, microstrip with conductors on one or both sides of the substrate, suspended stripline, and coplanar waveguide circuits. Of these, coplanar waveguide has two major advantages: (i) it allows the use of a relatively thick substrate (*e.g.*, 0.0035" for a 200-300 GHz mixer [4]), and (ii) with the center conductor and ground-plane on the same side of the substrate, transmission line dimensions can be kept small to minimize the parasitic inductance and capacitance associated with a series array of devices, which can ultimately limit the bandwidth of the circuit. A broadband transducer from coplanar waveguide to rectangular waveguide can be made using an intermediate section of suspended stripline, as described in [5].

In practical applications, a series array of devices may be preferable to a single device for two reasons. Firstly, for a given overall impedance

level, an array has greater power handling capacity and dynamic range than a single device. This can be an important benefit in frequency multipliers and mixers. Secondly, the devices in a series array are larger than a single device of the same impedance as the array. This can substantially reduce the difficulty of fabrication and result in better quality devices. The (theoretical) match bandwidth of an array of devices is only lower than that of the equivalent single device if the array is so long that the series inductance of the array exceeds the value L_B mentioned above; otherwise, the Bode limit predicts equal maximum bandwidths for the single device and the array. The SIS mixer examples below assume the simple coplanar array of junctions shown in Fig. 8, with physical dimensions chosen to give the lowest series inductance consistent with reproducible fabrication using standard photolithography.

For the circuit of Fig. 8, the series inductance depends on the number N_J of junctions. Fig. 9 shows the normalized series reactance $\omega L/R$ of the circuit as a function of the number of junctions in the array, with frequency as parameter. The resistance $R = N_J R_J$ is the small-signal RF resistance of the array. A quartz substrate, with $\epsilon_r = 3.8$, is assumed. At higher frequencies, and for larger numbers of junctions, the electrical length of the coplanar line becomes significant, as indicated by the curvature of the upper curves in Fig. 9, and the circuit can no longer be characterized accurately as an array of RC devices in series with a frequency-independent inductance. The values of $\omega L/R$ in Fig. 9 can be used with Fig. 5 to determine the upper (Bode/Fano) limit of the RF match bandwidth of this circuit. The horizontal dashed lines in Fig. 9 indicate the values of $\omega L/R$ above which the inductance of the array limits the achievable bandwidth, for $\omega RC = \omega R_J C_J = 2$, 4, and 8. For a given frequency of operation, the intersection of the appropriate solid curve with the dashed curve, corresponding to the given value of ωRC, indicates the cross-over from the Bode limit (due only to R and C) to the Fano limit. *These intersections also indicate the maximum number of junctions that can be used for a given ωRC without limiting the RF bandwidth.* If a smaller number of junctions is used, the first element of the optimum matching network is an additional inductance, and the Bode limit can, in principle, be attained.

For the circuit of Fig. 8, with only one or two junctions, it is possible to use inductive tuners on the individual junctions [6] to tune out their capacitance, as indicated in Fig. 10. In this case, the bandwidth limits of Fig. 6 apply. It is clear that, for $|\rho| \leq 0.2$ or 0.4, the series inductance does not limit the achievable bandwidth, and the Bode limit applies in most practical cases. Mixers described in [7-12] have successfully used one or two individually tuned junctions, though not in a coplanar transmission line circuit. The use of individual inductive tuners with more than two junctions is not possible for this simple coplanar circuit configuration without orienting the additional tuners perpendicular to the center conductor. This would introduce unacceptable capacitance between the tuners and the ground plane. To avoid this, the ground plane can be removed in the vicinity of the tuners. Such an approach has been successfully used in SIS mixers for 75-110 GHz [5] and 200-300 GHz [4], but the equivalent circuit is much more complicated [13], and this configuration will not be discussed further here.

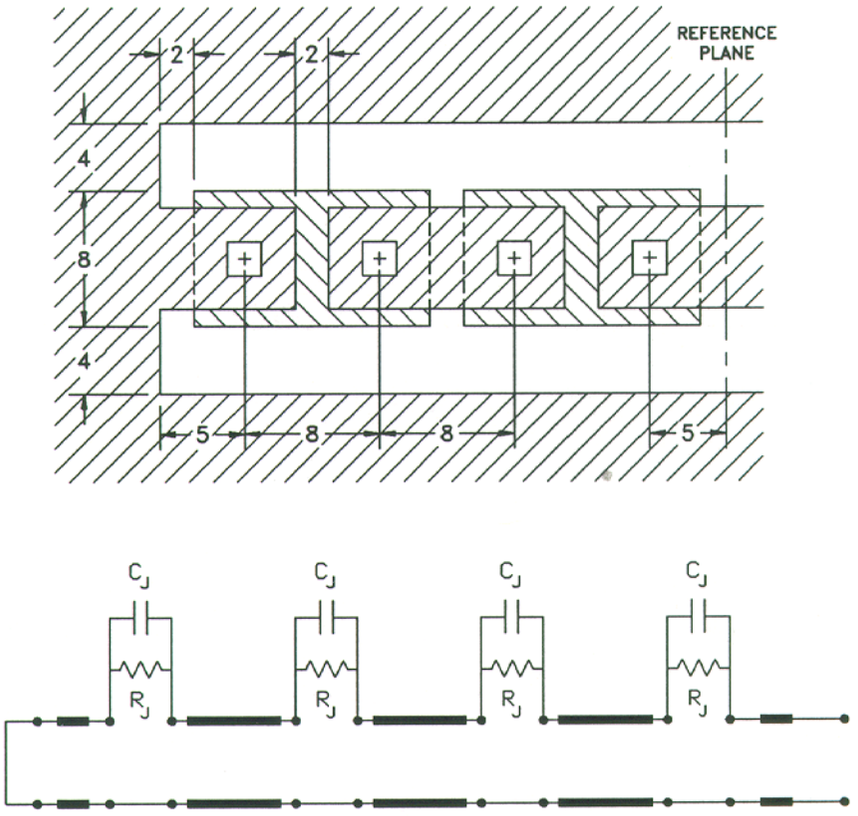

Fig. 8. Series array of SIS junctions in coplanar waveguide, and its equivalent circuit. The dimensions (shown in μm) are chosen to give the lowest series inductance consistent with reproducible fabrication using standard photolithography. The physical length of such an array of N_J junctions is $(8N_J+2)$ μm.

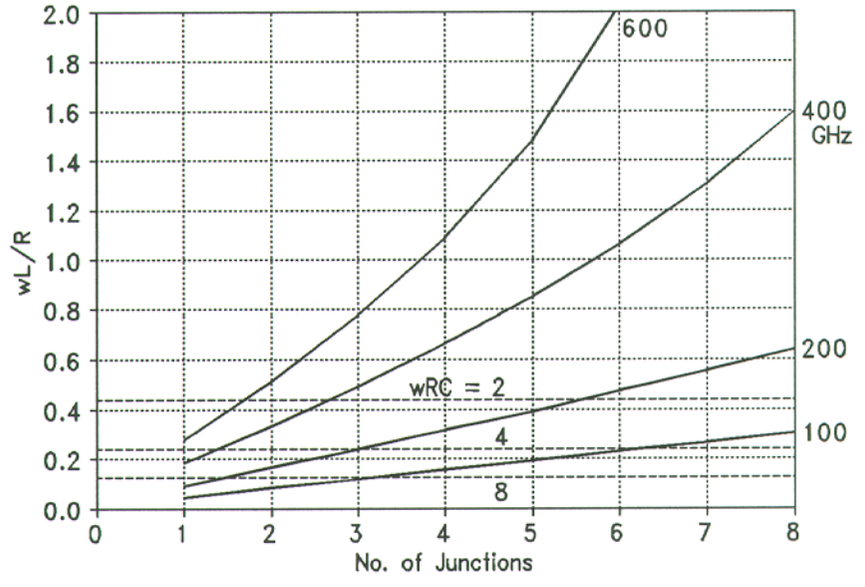

Fig. 9. Normalized series reactance $\omega L/R$ of arrays of SIS junctions in a coplanar waveguide with the dimensions shown in Fig. 8. A quartz substrate is assumed, with $\epsilon_r = 3.8$. The RF resistance of the array, R, is assumed to be 50 Ω. The curvature of the lines for larger arrays at higher frequencies is a result of the significant electrical length of the array. The horizontal dashed lines indicate the values of $\omega L/R$ above which the inductance of the array limits the achievable match-bandwidth, for $\omega RC = 2$, 4, and 8.

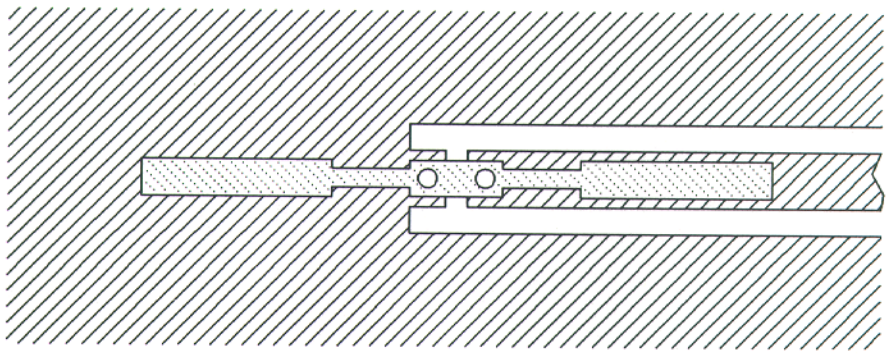

Fig. 10. A two-junction SIS mixer in coplanar waveguide, with inductive tuners on each junction.

The choice of the number of junctions in series, N_J, to use in an SIS mixer depends on two main factors: the desired dynamic range (or saturation power level), and the smallest size of junction that can be made with sufficient quality and reproducibility. For a given embedding impedance and critical current density J_C, the required junction area is proportional to N_J, so several minimum size junctions in series may be required to reach the desired embedding impedance level. The saturation power of an SIS mixer is proportional to ωN_J^2 [14], which may therefore govern the minimum value of N_J. As the series inductance of the SIS array increases with N_J, it follows that the designer may in some cases be faced with a trade-off between bandwidth and dynamic range: using more junctions in series to increase the saturation power will reduce the available RF bandwidth of the mixer if the series inductance of the array exceeds the value L_B.

VIII. An Example

Although the question of how closely the Bode and Fano bandwidth limits can be approached using practical circuits is outside the scope of the present work, it is informative to examine a realistic example. We choose a 250 GHz mixer with a coplanar array of SIS junctions, and a matching circuit of moderate complexity. A four junction coplanar array, as shown in Fig. 8, is connected to a matching network containing a series capacitor and four transmission lines in series, similar, except for the capacitor, to the tuning circuit described in [7]. The complete circuit is shown in Fig. 11. Note that the electrical length of the array of junctions is small, and the equivalent circuit of Fig. 1(b) is applicable. The capacitor C_A was initially adjusted to make the impedance of the SIS array real at the center frequency, lines 1, 2, and 3 were set to a quarter wavelength, and the fourth line set to half a wavelength. The microwave circuit design program MMICAD [15] was then used to optimize the elements of the matching network to give $|\rho| \leq 0.4$ over the widest possible bandwidth. The resulting embedding admittance is shown in Fig. 12 on an admittance Smith chart ($(-\rho)$-plane). The optimized values of the elements in the matching network are: $C_A = 75$ fF, $Z_{01} = 2.48\ \Omega$, $Z_{02} = 2.34\ \Omega$, $Z_{03} = 16.5\ \Omega$, $Z_{04} = 61.2\ \Omega$, $l_1 = 0.265\ \lambda_{g0}$, $l_2 = 0.246\ \lambda_{g0}$, $l_3 = 0.254\ \lambda_{g0}$, and $l_4 = 0.516\ \lambda_{g0}$.

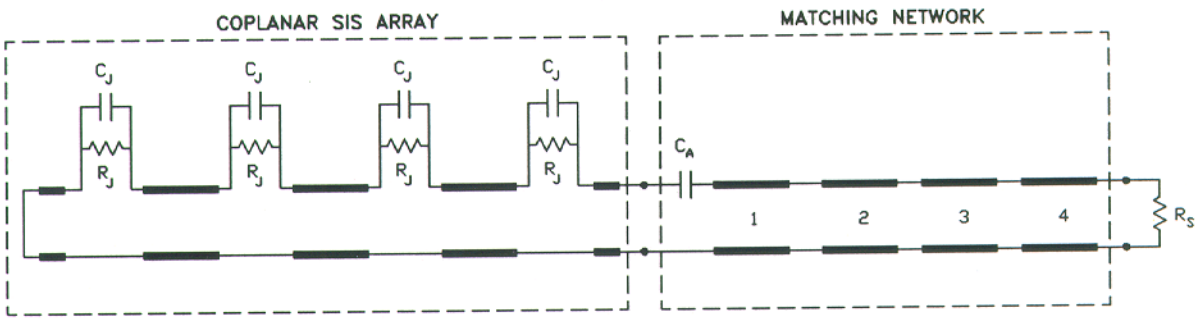

Fig. 11. Circuit of the 250 GHz SIS mixer used in the example. The coplanar SIS array is the same as in Fig. 8, and has four junctions of RF small-signal resistance $R_J = 12.5\ \Omega$, and $\omega RC = \omega R_J C_J = 4$. The matching network contains a capacitor C_A in series with four transmission line matching sections. The source resistance $R_S = 50\ \Omega$.

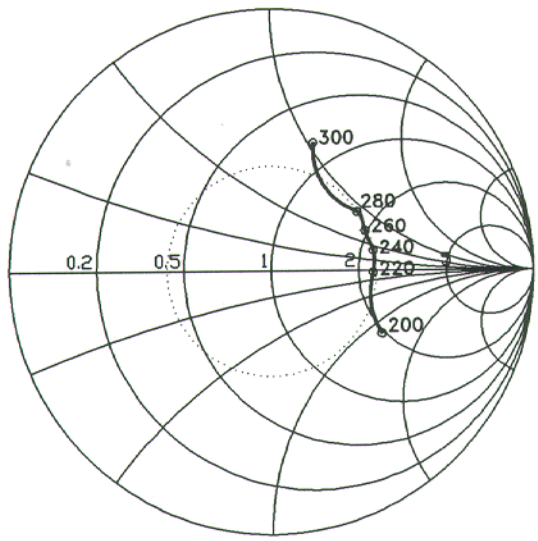

Fig. 12. Embedding admittance of the SIS mixer in Fig. 11 after optimizing the matching network to give the widest possible bandwidth with $|\rho| \leq 0.4$. Admittances are normalized to the RF conductance of the array $1/R = 1/4R_J$. The dotted circle is at $|\rho| = 0.4$.

The magnitude of the reflection coefficient $|\rho| \leq 0.4$ from 206-296 GHz, giving a fractional bandwidth b = 0.36. For comparison, the Fano bandwidth limit for the same mixer can be deduced from Fig. 5, using $\omega RC = 4$ and $\omega L/R = 0.4$ (from Fig. 9), and is $b_{Fano} = 0.55$. The Bode limit for SIS junctions with $\omega RC = 4$ is $b_{Bode} = 0.85$. The bandwidth for an inductively shunted junction (*i.e.*, with a parallel tuning inductor and no other matching

elements) and the same value of ωRC, is $b_{isj} = 0.22$. These numbers are listed in decreasing order in the table below:

Circuit	b
Bode limit for parallel RC	85%
Fano limit with series L	55%
Circuit of Fig. 11	36%
RC with parallel L tuning	22%

IX. Conclusion

The theoretical limit on the match bandwidth of the circuit of Fig. 1(b) was derived by Fano for the low-pass case, and thence for the band-pass case via the standard low-pass to band-pass mapping in which the inductors and capacitors are transformed into series and parallel LC resonators. When the terminals of the intrinsic device are not accessible, it is not possible to connect an inductor in parallel with C, and the low-pass to band-pass mapping cannot be used. Here, Fano's analysis has been extended to determine the theoretical limit on the match bandwidth of the circuit of Fig. 1(b) without using the frequency mapping. For the circuit of Fig. 1(c), the theory of Fano has been used, with the low-pass to band-pass frequency mapping, to determine the match bandwidth. For the circuit of Fig. 1(a), the theory of Bode was used.

For the equivalent circuits of Figs. 1(b) and (c), it is found that the series inductance L limits the match bandwidth only when it exceeds a value L_B, dependent on the other circuit elements. For values of L less than L_B, Bode's bandwidth limit is theoretically attainable, and there is no fundamental reason to make L smaller than L_B when designing a broadband circuit. We conclude that using a series array of N_J devices imposes no restriction on the theoretically attainable bandwidth of the circuit as long as N_J does not exceed the number for which the series inductance of the array is equal to L_B.

In circuits using series arrays of devices, the power handling capacity or saturation level depends on N_J^2. It is possible that in designing a broadband circuit, there will a conflict between power handling (requiring more devices) and bandwidth (requiring fewer devices) if the series inductance of the array exceeds L_B.

The relevance of the (RF) input match to the overall performance of double sideband mixer receivers is discussed using the example of a 250 GHz SIS mixer with typical niobium junctions. It is found that acceptable performance results if the input reflection coefficient $|\rho| \leq 0.4$. When the mixer is realized in a coplanar waveguide circuit, it is shown that a useful

bandwidth of 36% (comparable to a standard waveguide bandwidth) is achievable without the use of inductive tuning circuits on the individual junctions. A mixer with a simple inductively tuned junction (parallel RCL), but with no other matching elements, would have a bandwidth of 22%. These figures are to be compared to the maximum theoretical bandwidth of 55%.

X. Acknowledgements

The author would like to thank M. J. Feldman, J. Granlund, S.-K. Pan and M. W. Pospieszalski for their helpful discussions and comments on the manuscript.

XI. References

[1] H. W. Bode, "Network Analysis and Feedback Amplifier Design," New York: Van Nostrand, 1945.

[2] R. M. Fano, "Theoretical Limitations on the Broadband Matching of Arbitrary Impedances," *J. Franklin Inst.*, vol. 249, pp. 57-83 and 139-155, Jan. and Feb. 1950.

[3] Q. Ke and M. J. Feldman, "Optimum Source Conductance for High Frequency Superconducting Quasi-Particle Receivers," *IEEE Trans. Microwave Theory Tech.*, vol. MTT-41, no. 4, pp. 600-604, April 1993.

[4] A. R. Kerr, S.-K. Pan, A. W. Lichtenberger and D. M. Lea, "Progress on Tunerless SIS Mixers for the 200-300 GHz Band," *IEEE Microwave and Guided Wave Letters*, vol. 2, no. 11, pp. 454-456, Nov. 1992.

[5] A. R. Kerr, S.-K. Pan, S. Whiteley, M. Radparvar, and S. Faris, "A Fully Integrated SIS Mixer for 75-110 GHz," *IEEE Int. Microwave Symp. Digest*, pp. 851-854, May 1990.

[6] A. R. Kerr, S.-K. Pan, and M. J. Feldman, "Integrated Tuning Elements for SIS Mixers," *Int. J. Infrared Millimeter Waves*, vol. 9, no. 2, pp. 203-212, Feb. 1988. This paper was presented at the International Superconductivity Electronics Conference, Tokyo, Japan, Aug. 1987.

[7] G. Pance and M. J. Wengler, "Integrated Tuning Elements for Millimeter and Submillimeter SIS Mixers," *IEEE International Microwave Symposium Digest*, pp. 337-340, June 1992.

[8] G. Pance and M. J. Wengler, "Broadband Quasi-Optical SIS Mixers with Large Area Junctions," *Proceedings of the Fourth International Symposium on Space Terahertz Technology*, pp. 652-660, March 1993.

[9] F. Schafer, E. Kreysa, T. Lehnert, and K. H. Gundlach, "A Planar SIS Receiver with Log-Periodic Antenna for Submillimeter Waves," *Proceedings of the Fourth International Symposium on Space Terahertz Technology*, pp. 661-665, March 1993.

[10] A. Karpov, M. Carter, B. Lazareff, M. Voss, D. Billon-Peron, K. H. Gundlach, "Wideband Fixed-Tuned and Tuneable SIS Mixers for 230 GHz and 345 GHz Receivers," Proceedings of the Fourth International Symposium on Space Terahertz Technology, p. 11, March 1993.

[11] W. R. McGrath, P. Febvre, P. Batelaan, H. G. LeDuc, B. Bumble, M. A. Frerking and J. Hernichel, "A Submillimeter Wave SIS Receiver for 547 GHz," *Proceedings of the Fourth International Symposium on Space Terahertz Technology*, pp. 50-58, March 1993.

[12] J. Mees, A. Skalare, M. M. T. M. Dierichs, H. van der Stadt, R. A. Panhuyzen, Th. de Graauw, and T. M. Klapwijk, "Double Dipole Antenna SIS Receivers at Frequencies Above 500 GHz," *Proceedings of the Fourth International Symposium on Space Terahertz Technology*, pp. 59-71, March 1993.

[13] A. R. Kerr, S.-K. Pan and N. J. Bailey, "The Embedding Impedance in SIS Mixers and Other Circuits Using Compact and Distributed Arrays of Identical Devices," in preparation.

[14] M. J. Feldman, S.-K. Pan and A. R. Kerr, "Saturation of the SIS Mixer," International Superconductivity Electronics Conference, Tokyo, *Digest of Technical Papers*, pp. 290-292, Aug. 1987.

[15] MMICAD is a microwave integrated circuit analysis and optimization program, and is a product of Optotek, Ltd., Ontario, Canada K2K-2A9.

[16] A. R. Kerr and S.-K. Pan, "Some Recent Developments in the Design of SIS Mixers," *Int. J. Infrared Millimeter Waves*, vol. 11, no. 10, pp. 1169-1187, Oct. 1990.

[17] A. R. Kerr, S.-K. Pan and S. Withington, "Embedding Impedance Approximations in the Analysis of SIS Mixers," *IEEE Trans. Microwave Theory Tech.*, vol. 41, no. 4, April 1993. This paper was originally presented at the Third International Symposium on Space Terahertz Technology, March 1992.

APPENDIX: Details of the "Typical" SIS Mixer Used in the Simulations

The mixer is assumed to be designed according to the procedure described in [16], modified as in [4], in which the optimum signal and image source and IF load impedances are all equal to $R_{S,opt} = (R_N/2.4)(100/f(GHz))^{0.72}$, where R_N is the normal resistance of the junction (or array of junctions). The mixer is analyzed using the quasi five-frequency approximation [17] to Tucker's theory, and the I-V curve, shown in Fig. A-1, for four Nb/Al-Al_2O_3/Nb junctions in series. The pumping parameter $\alpha = eV_{LO}/\hbar\omega_{LO} = 1.2$, and the DC bias voltage is at the mid-point of the first photon step. $\omega R_N C = 4$ at 230 GHz.

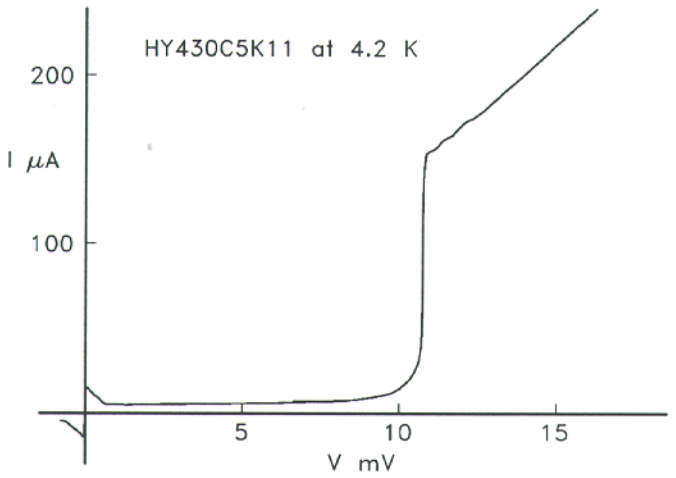

Fig. A-1. I-V curve used in the analysis (from [16]).